ELSEVIER

Polymer 43 (2002) 3047–3059

polymer

www.elsevier.com/locate/polymer

Temperature–composition phase diagrams of binary blends of block copolymer and homopolymer

Nitin Y. Vaidya, Chang Dae Han*

Department of Polymer Engineering, The University of Akron, Akron, OH 44325-0301, USA

Received 15 October 2001; received in revised form 10 January 2002; accepted 14 January 2002

Abstract

The temperature–composition phase diagrams for six pairs of diblock copolymer and homopolymer are presented, putting emphasis on the effects of block copolymer composition and the molecular weight of added homopolymers. For the study, two polystyrene-*block*-polyisoprene (SI diblock) copolymers having lamellar or spherical microdomains, a polystyrene-*block*-polybutadiene (SB diblock) copolymer having lamellar microdomains, and a series of polystyrene (PS), polyisoprene (PI), and polybutadiene (PB) were used to prepare SI/PS, SI/PI, SB/PS, and SB/PB binary blends, via solvent casting, over a wide range of compositions. The shape of temperature–composition phase diagram of block copolymer/homopolymer blend is greatly affected by a small change in the ratio of the molecular weight of added homopolymer to the molecular weight of corresponding block ($M_{H,A}/M_{C,A}$ or $M_{H,B}/M_{C,B}$) when the block copolymer is highly asymmetric in composition but only moderately even for a large change in $M_{H,A}/M_{C,A}$ ratio when the block copolymer is symmetric or nearly symmetric in composition. The boundary between the mesophase (M_1) of block copolymer and the homogeneous phase (H) of block copolymer/homopolymer blend was determined using oscillatory shear rheometry, and the boundary between the homogeneous phase (H) and two-phase liquid mixture ($L_1 + L_2$) with L_1 being disordered block copolymer and L_2 being macrophase-separated homopolymer was determined using cloud point measurement. It is found that the addition of PI to a lamella-forming SI diblock copolymer or the addition of PB to a lamella-forming SB diblock copolymer gives rise to disordered micelles (DM) having *no* long-range order, while the addition of PS to a lamella-forming SB diblock copolymer retains lamellar microdomain structure until microdomains disappear completely. Thus, the phase diagram of SI/PI or SB/PB blends looks more complicated than that of SI/PS or SB/PS blends.

Keywords: Block copolymer; Disordered micelles; Two-phase liquid mixtures

1. Introduction

A number of research groups carried out experimental [1–25] and theoretical [26–34] investigations on binary blends of a block copolymer and a homopolymer. Specifically, some research groups [1–15] carried out experimental investigations on microdomain structures, others [16–21] on phase transitions, and still others [18–25] on phase equilibria in binary blends of a block copolymer and a homopolymer. This subject is of practical and fundamental importance to polymer scientists. For example, blends of polystyrene-*block*-polyisoprene-*block*-polystyrene (SIS triblock) copolymer or polystyrene-*block*-polybutadiene-*block*-polystyrene (SBS triblock) copolymer with a tackifying resin (e.g. C5 aliphatic or C9 aromatic hydrocarbon resin) are used to produce pressure-sensitive adhesives. In order to produce good pressure-sensitive adhesives, a tackifying resin must be miscible with the midblock of an SIS or SBS triblock copolymer. This means that a C5 aliphatic hydrocarbon resin or a C9 aromatic hydrocarbon resin must be miscible with the polyisoprene (PI) midblock of an SIS triblock copolymer or with the polybutadiene (PB) midblock of an SBS triblock copolymer. An excess amount of tackifying resin will form separate domains, decreasing tackification of the pressure-sensitive adhesives. Therefore, it is highly desirable to have phase diagrams for blends of an SIS or SBS triblock copolymer and a tackifying resin. Han and coworkers [18–20] reported temperature–composition phase diagrams for several pressure-sensitive adhesive formulations that consisted of a commercially available tackifying resin and commercial SIS or SBS triblock copolymers. A practical difficulty with using a commercial tackifying resin from the point of view of developing fundamental relationships in phase equilibria lies in that the chemical structure of a commercial tackifying resin is difficult to determine, because it consists of several ingredients. Thus, it is not possible to determine the molecular weight of a commercial tackifying resin and consequently one cannot investigate the effect of molecular parameters on the

* Corresponding author. Tel.: +1-330-972-6468; fax: +1-330-972-5720.
E-mail address: cdhan@uakron.edu (C.D. Han).

0032-3861/02/$ - see front matter
PII: S0032-3861(02)00093-9

phase behavior of block copolymer/homopolymer blends. In order to overcome this difficulty, blends of a block copolymer and a homopolymer with known chemical structure and molecular parameters must be used as model compounds.

When homopolymer A is added to an AB-type diblock copolymer (hereafter referred to as A-*block*-B copolymer) having spherical or cylindrical microdomains of block A, the added homopolymer may enter into (or may be solubilized in) the microdomains of block A, swelling the size of the microdomains, until reaching a solubility limit. The excess amount of added homopolymer A that cannot enter into the microdomains will form a separate phase, undergoing macrophase separation. Depending upon the solubility limit which determines the maximum amount of homopolymer that can be added before macrophase separation sets in, a morphological transition, for instance, from spherical microdomains to cylindrical microdomains or to lamellar microdomains can occur. It is also possible to encounter a phase inversion; that is, block A which formed cylindrical microdomains in the neat block copolymer, upon addition of a sufficient amount of homopolymer A, may form the matrix phase in which block B now forms cylindrical microdomains. On the other hand, when homopolymer B is added to an A-*block*-B copolymer having spherical or cylindrical microdomains of block A, the added homopolymer B may be mixed with the matrix phase, block B, of the block copolymer until reaching a solubility limit, at and above which any excess amount of added homopolymer B will form a separate phase, undergoing macrophase separation.

Today, it is well established that the addition of homopolymer A to an A-*block*-B copolymer changes the order–disorder transition (ODT) temperature (T_{ODT}) of the resulting (A-*block*-B)/A blend, which in turn is determined by several factors: (i) the molecular weight of block copolymer (M_C), (ii) the molecular weight of homopolymer ($M_{H,A}$ or $M_{H,B}$), (iii) the block copolymer composition (f), and (iv) the weight fraction ($w_{H,A}$) or volume fraction ($\phi_{H,A}$) of homopolymer A in the (A-*block*-B)/A blend. In spite of much research activity reported on block copolymer/homopolymer binary blends in the past, very few experimental studies have been reported on the effect of block copolymer composition on temperature–composition phase diagrams of block copolymer/homopolymer binary blends. In the present study, we have constructed experimental temperature–composition phase diagrams for six pairs of (A-*block*-B)/A and (A-*block*-B)/B binary blends with block copolymers having spherical or lamellar microdomain structure. In this paper, we present the highlights of our findings.

2. Experimental

2.1. Materials

Using standard anionic polymerization procedures, we synthesized two polystyrene-*block*-polyisoprene (SI diblock) copolymers and a series of polystyrenes (PS) and polyisoprenes (PI) with *sec*-butyllithium as initiator and cyclohexane as solvent. A polystyrene-*block*-polybutadiene (SB diblock) copolymer and a polybutadiene (PB), both having very high vinyl content, were supplied to us by Dr Adel Halasa at Goodyear Tire and Rubber Company. Membrane osmometry (Jupiter Instrument, Model 231) was used to determine the molecular weights of the block copolymers and homopolymers having the number-average molecular weight (M_n) higher than 1.0×10^4 g/mol, and vapor pressure osmometry (KNAUER Osmometers) was used to determine the molecular weights of homopolymers having M_n lower than 1.0×10^4 g/mol. Gel permeation chromatography (Waters) was used to determine the polydispersity indices (M_w/M_n) of the entire block copolymers and homopolymers employed in this study. Sample codes and the molecular characteristics of the block copolymers are given in Table 1, and sample codes and the molecular characteristics of the homopolymers are given in Table 2. Proton nuclear magnetic resonance spectroscopy was used to determine the composition of each block copolymer and the microstructures of the PI and PB blocks in the respective block copolymers and also the microstructure of the homopolymers, PI and PB. We found that the PI blocks in the two SI diblock copolymers (SI-7/29 and SI-7/8) and two polyisoprenes (PI-14 and PI-28) have ca. 94 wt% 1,4-addition and ca. 6% 3,4-addition with no detectable amount of 1,2-addition, and that the PB block of SB-9/8 and PB-12 have very high vinyl content (ca. 90% 1,2-addition).

2.2. Sample preparation

Binary blends consisting of SI or SB diblock copolymer and PS, PI, or PB were prepared by solvent casting. Table 3 gives a summary of the polymer blends prepared with information on the weight fraction of homopolymer A ($w_{H,A}$), molecular volume ratio of homopolymer to block copolymer (V_H/V_C), degree-of-polymerization ratio of homopolymer to block copolymer (Z_H/Z_C), and molecular weight ratio of homopolymer to the corresponding block copolymer

Table 1
Molecular characteristics of the diblock copolymers investigated in this study

Sample code	M_n (g/mol)[a]	M_w/M_n[b]	w_{PS}[c]	f_{PS}[d]	Z_C[e]	T_{ODT} (°C)
SB-9/8[f]	1.67×10^4	1.04	0.53	0.48	239	123
SI-7/29	3.56×10^4	1.03	0.19	0.16	503	135
SI-7/8	1.44×10^4	1.02	0.48	0.43	181	85

[a] The number-average molecular weight was measured using membrane osmometry.
[b] Polydispersity was measured using gel permeation chromatography.
[c] w_{PS} is the weight fraction of PS block in the copolymer.
[d] f_{PS} is the volume fraction of PS block in the copolymer at 25 °C.
[e] Degree-of-polymerization defined by $Z_C = M_{w,PS}/104.14 + M_{w,PB}/54.09$ for SB diblock copolymer and $Z_C = M_{w,PS}/104.14 + M_{w,PI}/68.11$ for SI diblock copolymer.
[f] PB block in the SB-9/8 contains 89% 1,2-addition.

Table 2
Molecular characteristics of homopolymers synthesized

Sample code	M_n (g/mol)	M_w/M_n [a]	Z_H [b]
PS-1 [c]	1.5×10^3	1.06	15
PS-2 [c]	1.9×10^3	1.06	19
PS-21 [d]	2.08×10^4	1.05	209
PI-14 [d]	1.41×10^4	1.02	211
PI-28 [d]	2.76×10^4	1.04	421
PB-12 [d,e]	1.12×10^4	1.09	226

[a] Polydispersity was measured using gel permeation chromatography.
[b] Z_H is degree-of-polymerization.
[c] The number-average molecular weight was measured using vapor pressure osmometry.
[d] The number-average molecular weight was measured using membrane osmometry.
[e] PB-12 contains 89% 1,2-addition.

($M_{H,A}/M_{C,A}$ or $M_{H,B}/M_{C,B}$). Samples were prepared by dissolving a predetermined amount of SI or SB diblock copolymer and PS, PB, or PI in toluene (10% of solid in solution) in the presence of 0.1 wt% antioxidant (Irganox 1010, Ciba-Geigy Group), and then slowly evaporating the toluene. The evaporation of toluene was carried out initially in a fume hood at room temperature for a week and then in a vacuum oven at 40 °C for 3 days. The last trace of solvent was removed by drying the samples in a vacuum oven at elevated temperature by gradually raising the oven temperature, sufficiently high enough to remove toluene without inducing phase transition. The drying of the samples was continued until there was no further change in weight. The specimens for rheological measurements and transmission electron microscopy (TEM) were annealed in a vacuum oven at predetermined temperatures, which varied from specimen to specimen. The thermal history of each specimen will be given in the figure captions.

2.3. Rheological measurement

A Rheometrics mechanical spectrometer (Model RMS 800) with parallel-plate fixture (25 mm diameter) was used to conduct: (i) isochronal dynamic temperature sweep experiments to monitor the storage and loss moduli (G' and G'') at a fixed angular frequency (ω) of 0.01 rad/s, and (ii) dynamic frequency sweep experiments in order to measure G' and G'' as functions of ω ranging from 0.01 to 100 rad/s at various temperatures in the heating process. Data acquisition was accomplished with the aid of a microcomputer interfaced with the rheometer. The temperature control was satisfactory to within ±1 °C. The strain was varied from 0.04 to 0.3% depending upon the measurement temperature, which was well within the linear viscoelastic range for the materials investigated. All experiments were

Table 3
Molecular parameters for diblock copolymer/homopolymer blends

Sample code	f_{PS} [a]	w_H [b]	V_H/V_C [c]	Z_H/Z_C [d]	$M_{H,A}/M_{C,A}$ [e] or $M_{H,B}/M_{C,B}$
(a) (SB-9/8)/(PS-21) blends	0.48		1.40	0.87	2.37
90/10 (SB-9/8)/(PS-21)		0.10			
83/17 (SB-9/8)/(PS-21)		0.17			
(b) (SB-9/8)/(PB-12) blends	0.48		0.78	0.98	1.50
90/10 (SB-9/8)/(PB-12)		0.10			
75/25 (SB-9/8)/(PB-12)		0.25			
65/35 (SB-9/8)/(PB-12)		0.35			
(c) (SI-7/29)/(PS-1) blends	0.19		0.04	0.03	0.21
80/20 (SI-7/29)/(PS-1)		0.20			
60/40 (SI-7/29)/(PS-1)		0.40			
43/57 (SI-7/29)/(PS-1)		0.57			
(d) (SI-7/29)/(PS-2) blends	0.19		0.05	0.04	0.26
83/17 (SI-7/29)/(PS-2)		0.17			
66/34 (SI-7/29)/(PS-2)		0.34			
(e) (SI-7/8)/(PI-14) blends	0.43		1.05	1.20	1.85
90/10 (SI-7/8)/(PI-14)		0.10			
75/25 (SI-7/8)/(PI-14)		0.25			
(f) (SI-7/8)/(PI-28) blends	0.43		2.10	2.40	3.69
90/10 (SI-7/8)/(PI-28)		0.10			
82/18 (SI-7/8)/(PI-28)		0.18			

[a] f_{PS} denotes the volume fraction of PS in the block copolymer.
[b] w_H denotes the weight fraction of added homopolymer in the blend.
[c] V_H/V_C denotes the molecular (or molar) volume ratio of added homopolymer to the block copolymer.
[d] Z_H/Z_C denotes the ratio of the degree-of-polymerization of added homopolymer to the degree-of-polymerization of block copolymer.
[e] $M_{H,A}/M_{C,A}$ denotes the molecular weight ratio of added homopolymer A to corresponding block of copolymer, and $M_{H,B}/M_{C,B}$ denotes the molecular weight ratio of added homopolymer B to corresponding block of copolymer.

conducted under a nitrogen atmosphere to preclude oxidative degradation of the specimens.

2.4. Cloud point determination

Cloud point was measured to determine the binodal curve of a given blend. In order to determine cloud point, we used two different apparatuses. For the (SI-7/29)/(PS-1) and (SI-7/29)/(PS-2) blends, we used an apparatus consisting of a He–Ne laser light source with the wavelength of 632.8 nm and a heating stage. The laser beam was collimated through a heating chamber with a 2 mm aperture. The temperature of the hot stage was controlled using a programmable temperature controller (Model CN-2012, Omega). The intensity of the laser beam was controlled by placing neutral density filters. The scattered light intensities at various scattering angles were detected by a one-dimensional silicon diode Reticon detector (Model 1460, OMA III, EG and G Princeton Applied Research). For all other blends, we used an apparatus which was similar to that described earlier, with the exception that the scattered light intensities were detected at a fixed scattering angle using a silicon photodiode detector (HC-220-01, Hamamatsu Company) and the analog output of the detector was converted to digital signals by an A/D converter, and stored in the memory of a personal computer.

For determination of cloud point, thin films of a block copolymer/homopolymer blend were cast from a 10 wt% solution in toluene on a 25 mm diameter coverslip. To preclude oxidative degradation, 0.5 wt% antioxidant (Irganox 1010, Ciba-Geigy Group) was added to the solution. The film was initially dried in a fume hood at room temperature and then under vacuum at 80 °C for 4 h for (SI-7/8)/PI blends and at 100 °C for 4 h for all other blends.

During the cloud point measurement, the sample was heated well above the cloud point which was roughly determined initially through a preliminary run. The heated sample was allowed to cool at a fixed rate and scattered intensities were recorded at different temperatures. For the (SI-7/29)/(PS-1) blends, the scattered light intensities at different values of scattering vector q were recorded at different temperatures, whereas for all other blends, the scattered light intensities at a fixed value of q were recorded at different temperatures. Depending on the sample we used three different cooling rates: (i) for blends with cloud points below 190 °C we used a cooling rate of 0.5 °C/min, (ii) for blends with cloud points in the range of 190–210 °C we used a cooling rate of 2 °C/min, and (iii) for blends with cloud points higher than 210 °C, we used a cooling rate of 5 °C/min, which reduced the exposure time of the polymer to high temperature. To ensure that there was no thermal degradation of the sample, cloud points were determined twice using the same sample. For cloud points below 210 °C, the values of cloud point determined during the two successive experiments using the same sample had a maximum difference of about ±1.5 °C in all cases, whereas for blends with cloud points above 210 °C, the difference in cloud points determined during the two successive experiments was up to ±5 °C. In this study, cloud point was determined by the temperature at which the scattered light intensity first showed a significant increase.

2.5. Transmission electron microscopy

TEM was conducted to investigate the morphology of neat block copolymers and their blends with PS, PI, or PB. The thermal histories of the specimens used will be given in the figure captions. The ultrathin sectioning was performed by cryoultramicrotomy at −100 °C, below the glass transition temperature of PI or PB, to attain the rigidity of the specimen, using a Reichert Ultracut S low-temperature sectioning system. A transmission electron microscope (JEM1200EX II, JEOL) operated at 120 kV was used to obtain micrographs of the specimens stained with osmium tetroxide vapor.

3. Results and discussion

3.1. The selection of the molecular weight of homopolymer

From an experimental point of view, it is of utmost importance to select the right range of molecular weights of homopolymer and block copolymer, in order to obtain a temperature–composition phase diagram over the entire range of blend compositions. This is because too low molecular weight of a homopolymer would continuously decrease the T_{ODT} of a block copolymer/homopolymer blend without inducing macrophase separation, whereas too high molecular weight of a homopolymer would rapidly increase the T_{ODT} of a block copolymer/homopolymer blend making the completion of a phase diagram over the entire range of blend compositions virtually impossible. Thus there exist very intricate relationships between the molecular weight of homopolymer A ($M_{H,A}$) and the molecular weight of block copolymer (M_C), between $M_{H,A}$ and block copolymer composition (say the volume fraction of block A, f_A), and between $M_{H,A}$ and the molecular weight of the corresponding block of copolymer ($M_{C,A}$). The above-mentioned considerations suggest that one must rely, though qualitatively, on a theoretical guideline for selecting the proper range of molecular weights of homopolymer that is to be blended with a given block copolymer. For such purposes, it is very helpful to estimate the threshold value of $M_{H,A}$ that begins to *increase* the T_{ODT} of a block copolymer/homopolymer blend above that of the neat block copolymer. Needless to say, such a threshold value of $M_{H,A}$ would depend on the composition of a block copolymer. In the present study, we used the theory due to Leibler and Benoit [26] to determine such a threshold value of $M_{H,A}$ for each block copolymer/homopolymer selected. It should be

pointed out that the Leibler–Benoit theory [26] predicts the spinodal temperature for microphase separation ($T_{s,micro}$) and not the T_{ODT} of an (A-*block*-B)/A or (A-*block*-B)/B blend and that $T_{s,micro} \neq T_{ODT}$, except for $f_A = 0.5$.

Fig. 1 shows plots of molecular volume (or molar volume) ratio of homopolymer and block copolymer ($V_{H,PS}/V_C$ or $V_{H,PI}/V_C$) versus the volume fraction of PS block (f_{PS}) of an SI diblock copolymer in the limit of very small volume fractions of homopolymer PS or PI in the blend ($\phi_H \rightarrow 0$), at which the addition of PS or PI neither increases nor decreases the $T_{s,micro}$ of the block copolymer. It should be mentioned that, earlier, Nojima and Roe [29] constructed plots of $V_{H,PS}/V_C$ versus f_{PS} for diene-based diblock copolymers. Note that $V_{H,PS}$ and $V_{H,PI}$ are the molecular (or molar) volumes of PS and PI, respectively, and V_C is the molar volume of an A-*block*-B copolymer. Referring to Fig. 1, curve 1 represents the threshold value of $V_{H,PS}/V_C$ ratio that neither increases nor decreases the $T_{s,micro}$ of the block copolymer when a PS is added to SI diblock copolymer, i.e. the $T_{s,micro}$ of an SI/PS blend will increase (or decrease) when the $V_{H,PS}/V_C$ ratio lies above (or below) curve 1. For example, for a given f_{PS} of an SI diblock copolymer having M_C, the $T_{s,micro}$ of an SI/PS blend will increase if $M_{H,PS}$ is chosen, such that the $V_{H,PS}/V_C$ ratio lies above curve 1. Thus, curve 1 in Fig. 1 indicates that as f_{PS} is increased, one must increase $M_{H,PS}$ (thus $V_{H,PS}$) in order to increase the $T_{s,micro}$ of an SI/PS blend above that of SI. Likewise, curve 2 in Fig. 1 indicates that as f_{PS} is decreased, one must increase $M_{H,PI}$ (thus $V_{H,PI}$) in order to increase the $T_{s,micro}$ of an SI/PI blend above that of SI. That is, when $M_{H,PS}$ or $M_{H,PI}$ is lower than a certain critical value, $T_{s,micro}$ will decrease by the addition of PS or PI to SI.

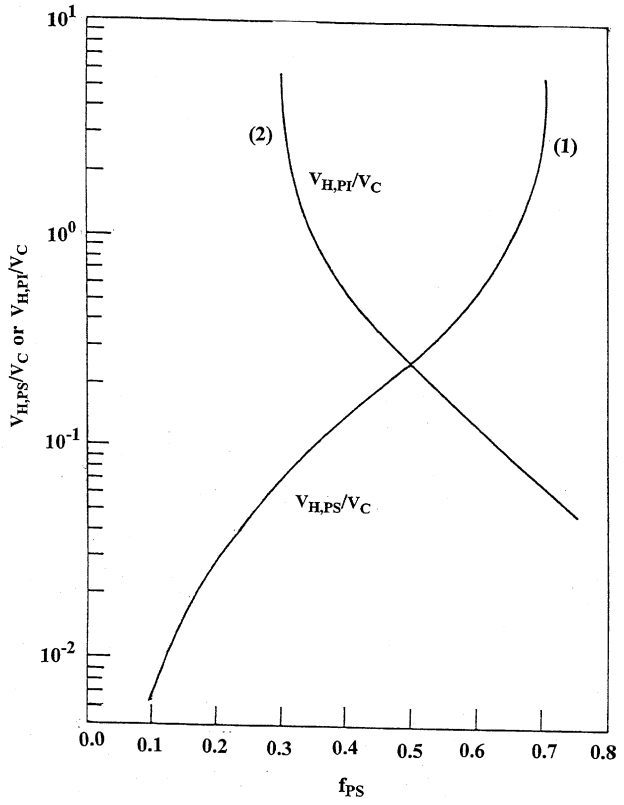

Fig. 1. The dependence of molecular volume ratio of added homopolymer (PS or PI) to block copolymer, $V_{H,PS}/V_C$ or $V_{H,PI}/V_C$, on the volume fraction of PS block (f_{PS}) in an SI diblock copolymer. Curve 1 describes the critical value of $V_{H,PS}/V_C$ at which the addition of PS to an SI diblock copolymer neither increases nor decreases the spinodal temperature (T_s) of the blend in the limit of zero concentration of added PS. Curve 2 describes the critical value of $V_{H,PI}/V_C$ at which the addition of PI to an SI diblock copolymer neither increases nor decreases the T_s of the blend in the limit of zero concentration of added PI. The values of $V_{H,PS}/V_C$ or $V_{H,PI}/V_C$ lying above curve 1 or curve 2 will increase the T_s of the binary blend in the limit of zero concentration of added homopolymer.

3.2. Temperature–composition phase diagram for (SB-9/8)/PS binary blends

Fig. 2 gives log G' versus log G'' plots, which Neumann et al. [35] referred to as the 'Han plot', for SB-9/8 at various temperatures ranging from 90 to 130 °C. According to the rheological criterion by Han et al. [36–38], the threshold temperature at which, during the dynamic frequency sweep experiments in the heating process, the Han plot having a slope of 2 in the terminal region becomes independent of temperature represents T_{ODT} for symmetric or nearly symmetric block copolymers. Following such a rheological

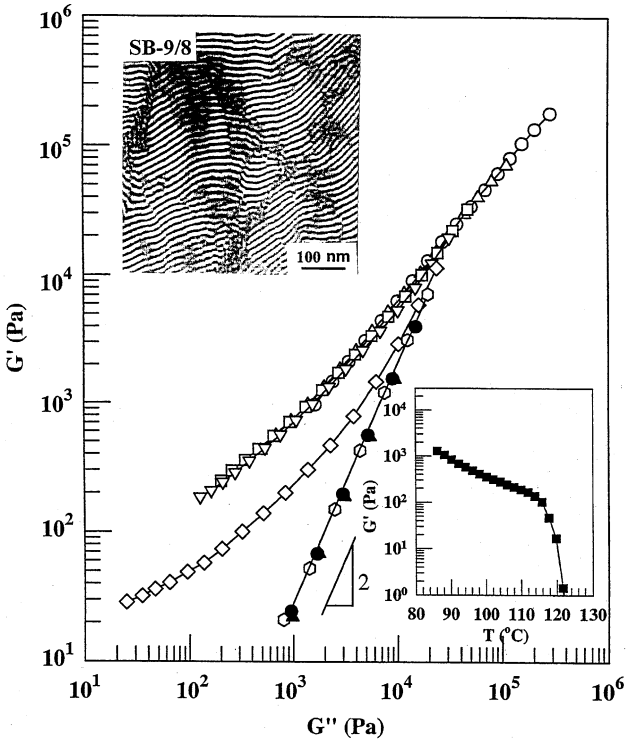

Fig. 2. Han plots for SB-9/8 at various temperatures: (○) 90 °C; (△) 100 °C; (□) 111 °C; (▽) 115 °C; (◇) 120 °C; (⬡) 123 °C; (●) 126 °C; (▲) 130 °C. The inset in the lower right corner gives the dependence of G' on temperature during the isochronal temperature sweep experiment at $\omega = 0.01$ rad/s in the heating cycle, and the inset in the upper left corner gives a TEM image of an SB-9/8 specimen taken at room temperature.

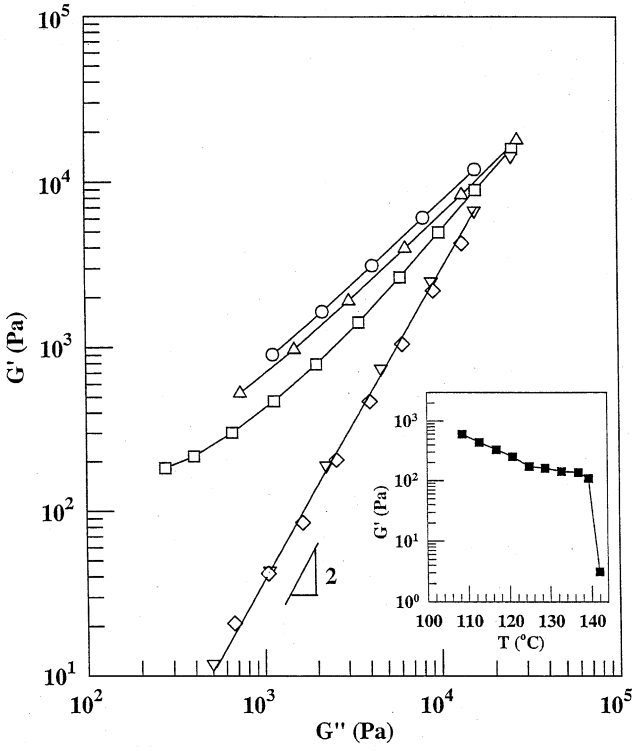

Fig. 3. Han plots for 90/10 (SB-9/8)/(PS-21) blend at various temperatures: (○) 122 °C; (△) 133 °C; (□) 138 °C; (▽) 141 °C; (◇) 146 °C. The inset in the lower right corner gives the dependence of G' on temperature during the isochronal temperature sweep experiment at $\omega = 0.01$ rad/s in the heating cycle. The specimen was annealed at 125 °C for 5 days.

criterion, from Fig. 2 we determine the T_{ODT} of SIB9/8 to be 123 °C. Notice in Fig. 2 that the Han plot is unchanged as the temperature is increased from 123 to 126 and to 130 °C. The theoretical basis that the Han plot remains independent of temperature for all homogeneous, single-phase polymeric liquids has been reported previously [39,40]. Also given in Fig. 2 are plots of log G' versus temperature that were obtained from the isochronal dynamic temperature sweep experiments for SB-9/8. Following the rheological criterion [41–43] that the temperature at which the value of G' begins to drop abruptly in the plot of log G' versus temperature signifies T_{ODT}, we determine the T_{ODT} of SB-9/8 to be ca. 118 °C, which is reasonably close to 123 °C determined from the Han plot. In our previous papers [44,45], we have shown that for symmetric or nearly symmetric block copolymers, the value of T_{ODT} determined from the Han plot agrees very well with that determined from the isochronal dynamic temperature sweep experiment. Indeed, SB-9/8 has lamellar microdomains as shown in the inset of Fig. 2.

Fig. 3 gives Han plots for the 90/10 (SB-9/8)/(PS-21) blend, from which we determine the T_{ODT} to be 141 °C. It is seen that the temperature dependence of the Han plot given in Fig. 3 is very similar to that given in Fig. 2 for the neat block copolymer, SB-9/8. Also given in Fig. 3 are plots of log G' versus temperature that were obtained from the isochronal dynamic temperature sweep experiments for

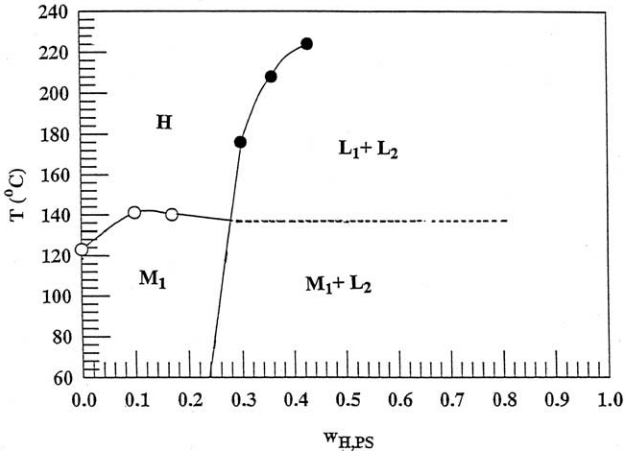

Fig. 4. Temperature–composition phase diagram for (SB-9/8)/(PS-21) blends, where H denotes the homogeneous phase in which disordered SB-9/8 chains and PS-21 chains are mixed on a molecular level, M_1 denotes a mesophase in which part of the added PS-21 is solubilized in the microdomains of SB-9/8, L_1 denotes disordered SB-9/8, and L_2 denotes macrophase-separated PS-21. The open circle ○ denotes T_{ODT} determined from the Han plot and the filled circle ● denotes cloud point determined from light scattering.

the 90/10 (SB-9/8)/(PS-21) blend, suggesting that $T_{ODT} \approx 140$ °C that is very close to that determined from the Han plot.

Fig. 4 shows a temperature–composition phase diagram for (SB-9/8)/(PS-21) binary blends, where H denotes the homogeneous phase in which disordered SB-9/8 chains and PS-21 chains are mixed on a molecular level, M_1 denotes the mesophase of SB-9/8 in which part of added PS-21 is solubilized, L_1 denotes disordered SB-9/8, and L_2 denotes macrophase-separated PS-21. The readers are reminded that SB-9/8 has a 0.48 volume fraction of PS block (Table 1), giving rise to lamellar microdomain structure (Fig. 2). It should be mentioned that the mesophase M_1 shown in Fig. 4 may have a microdomain structure other than lamellar microdomain structure, depending upon the amount of PS-21 solubilized. For instance, the addition of 20 wt% PS-21 to the lamella-forming diblock copolymer SB-9/8 might have induced an order–order transition from lamellae to cylindrical microdomains of PB phase in the PS matrix. The precise determination of the microdomain structure in the mesophase M_1 requires an elaborate investigation using small-angle X-ray scattering (SAXS), which is beyond the major thrust of the present study. The above statement also applies to other phase diagrams presented below. In Fig. 4, region ($M_1 + L_2$) represents a two-phase mixture where phases M_1 and L_2 coexist, and region ($L_1 + L_2$) represents a two-phase mixture where phases L_1 and L_2 coexist. The phase boundary between the ($M_1 + L_2$) and ($L_1 + L_2$) regions indicated by the dotted horizontal line in Fig. 4 is drawn with the stipulation that the mesophase M_1 in region ($M_1 + L_2$) would transform into the disordered phase (L_1), which coexists with macrophase-separated PS-21 phase (L_2). Again, the precise determination of the

temperatures separating the $(M_1 + L_2)$ and $(L_1 + L_2)$ regions requires an elaborate investigation using SAXS, which is beyond the major thrust of the present study. The phase boundary between the M_1 and $(M_1 + L_2)$ regions indicated by the solid vertical line in Fig. 4 is drawn on the basis of the results from the light scattering experiments indicating that macrophase separation occurred at 60 °C for a 0.24 weight fraction of PS-21.

The construction of the entire binodal curve in Fig. 4 was not possible, because the molecular weight of PS-21 was already too high, giving rise to significant thermal degradation/crosslinking reactions in the PB block of SB-9/8 at temperatures higher than about 220 °C. This result is not surprising in that $M_{H,PS}/M_{C,PS} = 2.37$ (Table 3) which is already high enough, limiting the solubility of PS-21 in SB-9/8. In Fig. 4, the boundary (denoted by the filled circle ●) between phases H and $(L_1 + L_2)$ was determined from cloud point measurements, and the boundary (denoted by the open circle ○) between phases H and M_1 was determined from T_{ODT} measurement.

3.3. Temperature–composition phase diagram for (SB-9/8)/PB binary blends

Fig. 5 gives Han plots for 90/10 (SB-9/8)/(PB-12) blend at various temperatures ranging from 85 to 156 °C. Notice that the temperature dependence of Han plot for the (SB-9/8)/(PB-12) blend shown in Fig. 5 is quite different from that observed in Fig. 3 for the 90/10 (SB-9/8)/(PS-21) blend in that the Han plot for the (SB-9/8)/(PB-12) blend begins to have a parallel feature at ca. 101 °C and begins to be independent of temperature at 151 °C. Similar results were obtained, although not presented here, for 75/25 and 65/5 (SB-9/8/(PB-12) blends. Following the interpretation given in our recent paper [45], from Fig. 5 we determine the lattice disordering/ordering transition (LDOT) temperature (T_{LDOT}) to be 101 °C and the demicellization/micellization transition (DMT) temperature (T_{DMT}) to be 151 °C for the 90/10 (SB-9/8)/(PB-12) blend. That is, disordered micelles (DM) exist between T_{LDOT} and T_{DMT}. It should be pointed out that the temperature at which the value of G' begins to drop precipitously at 104 °C in the plot of log G' versus temperature (see the inset of Fig. 5) almost coincides with the temperature at which the Han plot begins to have a parallel feature at 101 °C. Thus, we conclude that the isochronal dynamic temperature sweep experiment for the 90/10 (SB-9/8)/(PB-12) blend enables us to determine T_{LDOT} and not T_{DMT}. This conclusion is quite different from the conclusion drawn for the neat block copolymer SB-9/8, which is nearly symmetric, lamella-forming diblock copolymer (Fig. 2).

Fig. 6 shows a temperature–composition phase diagram for (SB-9/8)/(PB-12) binary blends, where H denotes the homogeneous phase in which disordered SB-9/8 chains and PB-12 chains are mixed on a molecular level, the symbol ○ represents the boundary between phase H and DM, and the symbol △ represents the boundary between

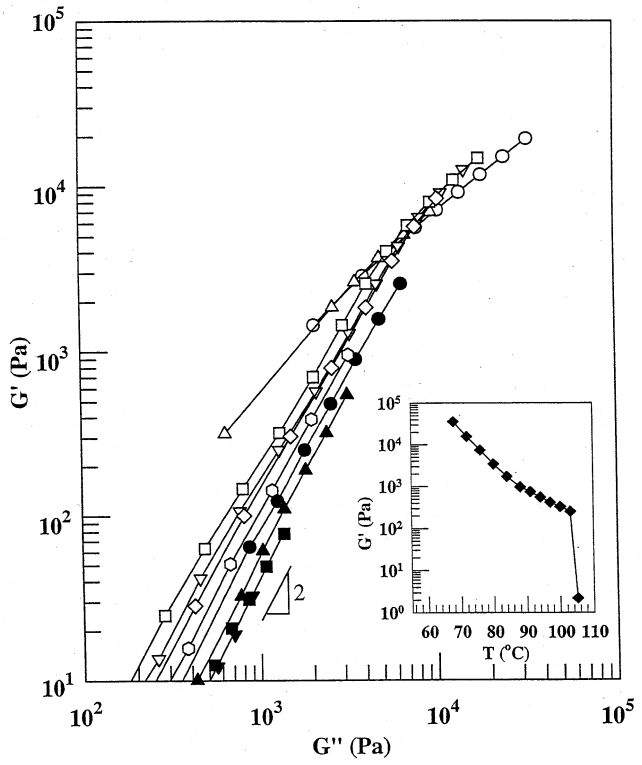

Fig. 5. Han plots for 90/10 (SB-9/8)/(PB-12) blend at various temperatures: (○) 85 °C; (△) 93 °C; (□) 101 °C; (▽) 104 °C; (◇) 111 °C; (⬡) 121 °C; (●) 131 °C; (▲) 141 °C; (■) 151 °C; (▼) 156 °C. The inset in the lower right corner gives the dependence of G' on temperature during the isochronal temperature sweep experiment at $\omega = 0.01$ rad/s in the heating cycle. The specimen was annealed at 90 °C for 4 days.

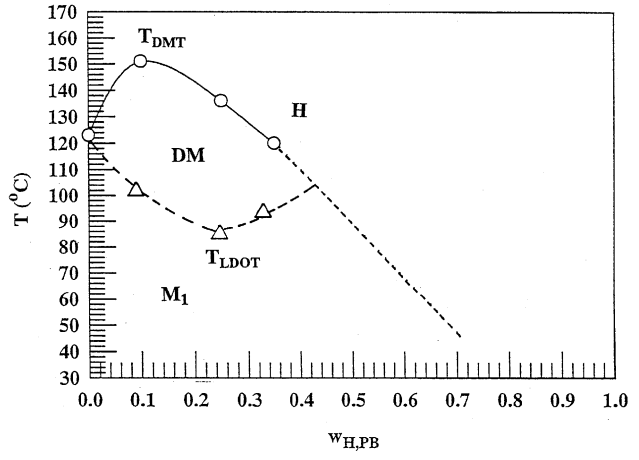

Fig. 6. Temperature–composition phase diagram for (SB-9/8)/(PB-12) blends, where H denotes the homogeneous phase in which disordered SB-9/8 chains and PB-12 chains are mixed on a molecular level, DM denotes disordered micelles, and M_1 denotes a mesophase in which part of the added PB-12 is solubilized in the microdomains of SB-9/8. The symbol ○ denotes T_{DMT} and the symbol △ denotes T_{LDOT}. No evidence of macrophase separation was observed over the entire range of blend compositions.

phases M_1 and DM, where M_1 denotes the mesophase of SB-9/8 in which added PB-12 is solubilized. It should be mentioned that the mesophase M_1 shown in Fig. 6 may have a microdomain structure other than lamellar microdomain structure, depending upon the amount of PB-12 solubilized. The addition of PB-12 to the lamella-forming diblock copolymer SB-9/8 might have induced an order–order transition from lamellae to cylindrical microdomains and then to spherical microdomains of PS phase in the PB matrix, depending upon the amount of PB-12 solubilized. Since the molecular weight ($M_n = 1.12 \times 10^4$ g/mol) of added PB-12 is much higher than the molecular weight ($M_n = 7.85 \times 10^3$ g/mol) of PB block in SB-9/8, we expect that the addition of PB-12 to SB-9/8 will *initially* increase the T_{DMT} of (SB-9/8)/(PB-12) blends above the T_{ODT} of SB-9/8.

3.4. Temperature–composition phase diagram for (SI-7/29)/PS binary blends

Fig. 7 gives Han plots for SI-7/29 blend at various temperatures ranging from 60 to 145 °C, showing that the Han plot begins to have a parallel feature at ca. 98 °C and begins to be independent of temperature at 135 °C. Similar results were obtained, although not presented here, for (SI-7/29)/(PS-1) and (SI-7/29)/(PS-2) blends. Following the interpretation given in our recent paper [45], from Fig. 7 we determine T_{LDOT} to be 98 °C and T_{DMT} to be 135 °C for SI-7/29. In a previous paper [45], we have reported via SAXS in the heating process that SI-7/29 first undergoes LDOT at 93–96 °C, forming DM, and then DMT at 130–135 °C, at which the DM disappears transforming into the micelle-free homogeneous state. It should be pointed out that the temperature at which the value of G' begins to drop precipitously at 98 °C in the plot of $\log G'$ versus temperature (see the inset of Fig. 7) coincides with the temperature at which the Han plot begins to have a parallel feature at 98 °C. Thus we conclude that the isochronal dynamic temperature sweep experiment for highly asymmetric, sphere-forming block copolymer enables us to determine T_{LDOT} and not T_{DMT}. This conclusion is quite different from the conclusion drawn for the nearly symmetric, lamella-forming block copolymer SB-9/8 (Fig. 2).

Fig. 8 shows a temperature–composition phase diagram for (SI-7/29)/(PS-1) binary blends, where H denotes the homogeneous phase in which disordered SI-7/29 chains and PS-1 chains are mixed on a segmental level, DM denotes disordered micelles, M_1 denotes the mesophase of block copolymer SI-7/29 in which part of added PS-1 solubilized, and L_2 denotes the macrophase-separated PS-1. The readers are reminded that SI-7/29 has a 0.16 volume fraction of PS block (Table 1), giving rise to spherical microdomains of PS phase (Fig. 7). It should be mentioned that the mesophase M_1 shown in Fig. 8 may have a microdomain structure other than spherical microdomain structure, depending upon the amount of PS-1 solubilized. That is, the addition of PS-1

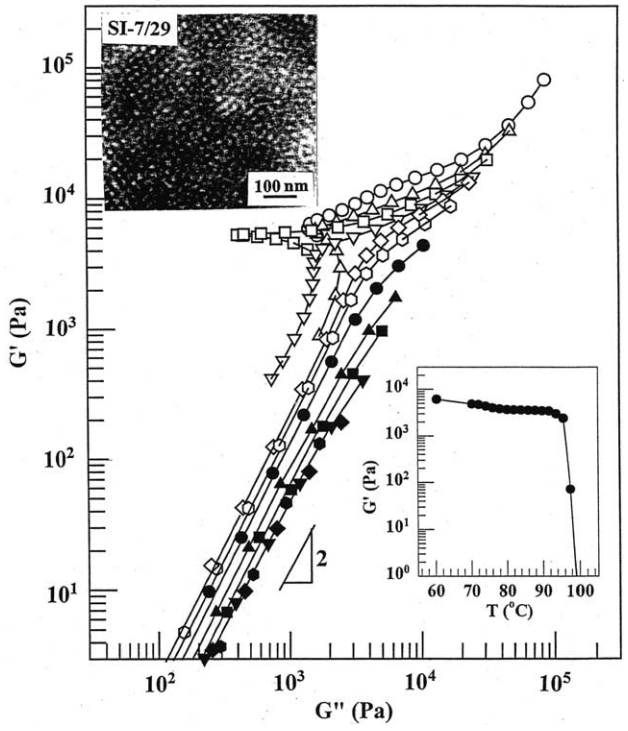

Fig. 7. Han plots for (SI-7/29) at various temperatures: (○) 60 °C; (△) 80 °C; (□) 90 °C; (▽) 96 °C; (◇) 98 °C; (⬡) 105 °C; (●) 115 °C; (▲) 125 °C; (■) 130 °C; (▼) 135 °C; (◆) 140 °C; (⬢) 145 °C. The inset in the lower right corner gives the dependence of G' on temperature during the isochronal temperature sweep experiment at $\omega = 0.01$ rad/s in the heating cycle, and the inset in the upper left corner gives a TEM image of an SI-7/29 specimen annealed at 60 °C for 12 days. The specimen used for dynamic temperature sweep experiment was annealed in a vacuum oven at 90 °C for 15 days and the specimen used for dynamic frequency sweep experiment was annealed in a vacuum oven at 70 °C for 2 days.

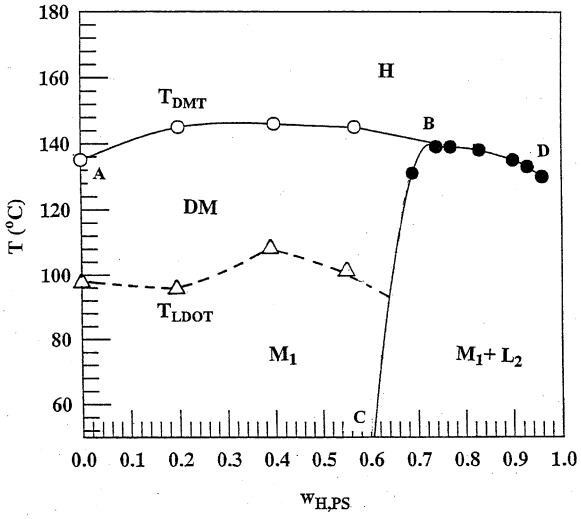

Fig. 8. Temperature–composition phase diagram for (SI-7/29)/(PS-1) blends, where H denotes the homogeneous phase in which disordered SI-7/29 chains and PS-1 chains are mixed on a molecular level, M_1 denotes a mesophase in which part of the added PS-1 is solubilized in the microdomains of SI-7/29, L_2 denotes macrophase-separated PS-1, and DM denotes disordered micelles. The symbol ○ denotes T_{DMT}, the symbol △ denotes T_{LDOT}, and the symbol ● denotes cloud point.

to the sphere-forming diblock copolymer SI-7/29 might have induced an order–order transition from body-centered cubic lattice of PS spheres to cylindrical microdomains of PS phase in the PI matrix and then to lamellar microdomain structure, depending upon the amount of PS-1 solubilized. The phase boundary between the M_1 and (M_1 + L_2) regions indicated by the solid vertical line in Fig. 8 is drawn on the basis of our light scattering experimental observation that macrophase separation occurred at 50 °C for a 0.6 weight fraction of PS-1. In Fig. 8, the symbol ○ represents T_{DMT} separating the boundary between phases H and DM, and the symbol △ represents T_{LDOT} separating the boundary between phases M_1 and DM. It should be mentioned that T_{LDOT} and T_{DMT} were determined from the Han plots for 80/20, 60/40, and 40/60 (SI-7/29/(PS-1) blends, not presented here, for the reason of space limitations. We observe that upon addition of PS-1 to SI-7/29, the T_{DMT} of the resulting blend initially increases gradually and then decreases slightly with a further increase in PS-1, before meeting the binodal curve at B.

Fig. 9(a) gives a TEM image of 80/20 (SI-7/29)/(PS-1) blend. Note that the addition of 20 wt% PS-1 to SI-7/29 increases the total weight fraction of PS in the binary mixture (w_{PS}^{T}) to 0.36, and thus caused a change in the size and/or shape of the microdomains. According to the phase diagram shown in Fig. 8, the entire amount of 20 wt% PS-1 added is solubilized in the spherical microdomains of SI-7/29 without inducing macrophase separation. Note that the addition of 40 wt% PS-1 to SI-7/29 increases w_{PS}^{T} to 0.51, which is sufficiently high to have caused a morphological transition in the resulting 60/40 (SI-7/29)/(PS-1) blend, as shown in Fig. 9(b). According to the phase diagram shown in Fig. 8, the entire amount of 40 wt% PS-1 added is solubilized in the spherical microdomains of SI-7/29. Fig. 9(c) gives a TEM image of 43/57 (SI-7/29)/(PS-1) blend, showing lamellar microdomains of PS. Note that the addition of 57 wt% PS-1 to SI-7/29 increases w_{PS}^{T} to 0.66, which is sufficiently high to have caused a morphological transition in the resulting 43/57 (SI-7/29)/(PS-1) blend. Again, according to the phase diagram shown in Fig. 8, the entire amount of 57 wt% PS-1 added is solubilized in the spherical microdomains of SI-7/29 without inducing macrophase separation. Fig. 9(d) gives a TEM image of 20/80 (SI-7/29)/(PS-1) blend. Note that the addition of 80 wt% PS-1 to SI-7/29 increases w_{PS}^{T} to 0.84, which exceeds the solubility limit and thus induces macrophase separation of PS-1. This is reflected in Fig. 9(d), showing that the morphology of the 20/80 (SI-7/29)/(PS-1) blend consists of the mesophase (the dark areas) of SI-7/29 and macrophase-separated PS-1 (the bright areas). Owing to low magnification of the TEM image, in Fig. 9(d), the details of microdomains is not discernible.

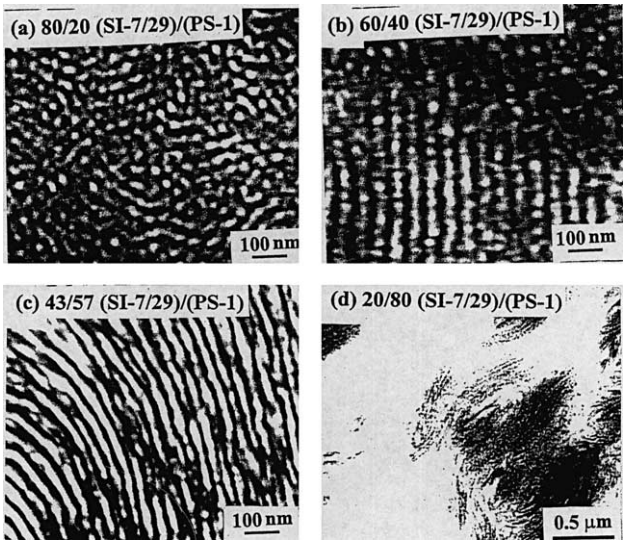

Fig. 9. TEM images of (SI-7/29)/(PS-1) blends: (a) 80/20 (SI-7/29)/(PS-1) blend annealed at 83 °C for 15 days; (b) 60/40 (SI-7/29)/(PS-1) blend annealed at 100 °C for 10 days; (c) 43/57 (SI-7/29)/(PS-1) blend annealed at 100 °C for 10 days; (d) 20/80 (SI-7/29)/(PS-1) blend annealed at 100 °C for 10 days.

Fig. 10 gives a temperature–composition phase diagram for (SI-7/29)/(PS-2) binary blends, where H denotes the homogeneous phase in which the disordered SI-7/29 chains and PS-2 chains are mixed on a segmental level, DM denotes disordered micelles, M_1 denotes the mesophase of block copolymer SI-7/29 in which part of the added PS-2 is solubilized in PS rich microdomains, L_1 denotes disordered SI-7/29, and L_2 denotes the macrophase-separated PS-2 rich phase. It should be mentioned that the mesophase M_1 shown in Fig. 10 may have a microdomain structure other than the spherical microdomain structure of SI-7/29, depending upon the amount of PS-2 solubilized. For instance, the addition of 17 wt% PS-2 to the sphere-forming diblock copolymer SI-7/

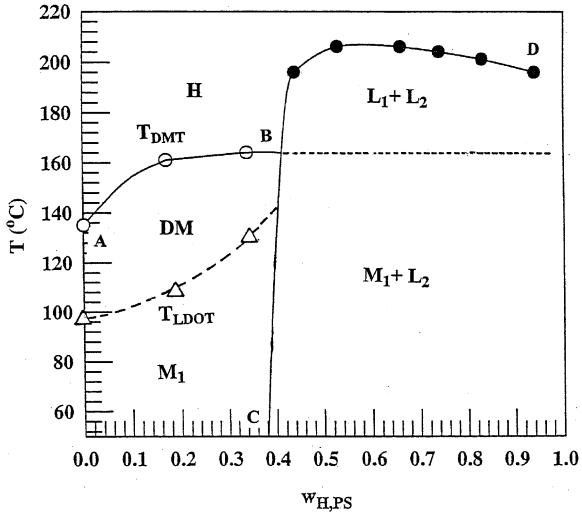

Fig. 10. Temperature–composition phase diagram for (SI-7/29)/(PS-2) blends, where H denotes the homogeneous phase in which disordered SI-7/29 and PS-2 are mixed on a molecular level, M_1 denotes a mesophase in which part of the added PS-2 is solubilized in the microdomains of SI-7/27, L_1 denotes disordered SI-7/29, L_2 denotes macrophase-separated PS-2, and DM denotes disordered micelles. The symbol ○ denotes T_{DMT}, the symbol △ denotes T_{LDOT}, and the symbol ● denotes cloud point.

29 might have induced an order–order transition from body-centered cubic lattice of PS spheres to cylindrical microdomains of PS phase in the PI matrix. In Fig. 10, region ($M_1 + L_2$) represents a two-phase region where phases M_1 and L_2 coexist, and region ($L_1 + L_2$) represents a two-phase region where phases L_1 and L_2 coexist. The phase boundary between the ($M_1 + L_2$) and ($L_1 + L_2$) regions indicated by the dotted horizontal line in Fig. 10 is drawn with the stipulation that the mesophase M_1 in the region ($M_1 + L_2$) would transform into the disordered phase (L_1), which coexists with macrophase-separated PS-2 phase (L_2). Again, the precise determination of the temperatures separating the ($M_1 + L_2$) and ($L_1 + L_2$) regions requires an elaborate investigation using SAXS, which is beyond the major thrust of the present study. The phase boundary between the M_1 and ($M_1 + L_2$) regions indicated by the solid vertical line in Fig. 10 is drawn on the basis of our light scattering experimental observation that macrophase separation occurred at 50 °C for a 0.38 weight fraction of PS-2.

Notice in Fig. 10 that (SI-7/29)/(PS-2) binary blends form DM before macrophase separation occurs, and that as the amount of added PS-2 is increased further, the T_{DMT} of (SI-7/29)/(PS-2) binary blends initially increases rapidly and then tends to level off before meeting the binodal curve at B. Notice that the onset of the binodal curve in Fig. 10 for (SI-7/29/(PS-2) blends occurs at $w_{H,PS} \approx 0.38$, which is lower than that in Fig. 8 for (SI-7/29/ (PS-1) blends. This is attributable to the fact that the molecular weight of PS-2 is higher than that of PS-1 (Table 2), and thus the solubility limit of PS-2 in SI-7/29 is less than that of PS-1 in SI-7/29. Comparison of Fig. 10 with Fig. 8 indicates that a relatively small increase in molecular weight (M_n) from 1.5×10^3 to 1.9×10^3 g/mol of added PS has increased considerably the critical temperature of (SI-7/29)/PS binary blends from ca. 140 to ca. 210 °C, i.e. the temperature–composition phase diagram is very sensitive to the molecular weight of added PS to SI-7/29 having spherical microdomains.

3.5. Temperature–composition phase diagram for (SI-7/8)/PI binary blends

Fig. 11 gives Han plots for SI-7/8 at various temperatures ranging from 76 to 96 °C, showing that SI-7/8 has T_{ODT} of 85 °C that is very close to the temperature at which G' begins to drop rapidly from the isochronal dynamic temperature sweep experiment (see the inset). This is as expected, because SI-7/8 has lamellar microdomains as shown in the inset of Fig. 11, similar to SB-9/8 also having lamellar microdomain structure (Fig. 2).

Fig. 12 gives Han plots for 90/10 (SI-7/8)/(PI-14) blends at various temperatures ranging from 60 to 125 °C, showing that it first undergoes LDOT at 80 °C and then DMT at 114 °C, very similar to that shown in Fig. 5 for the 90/10 (SB-9/8)/(PB-12) blend. Note that the temperature dependence of the Han plot for 90/10 (SI-7/8)/(PI-14) blend given in Fig. 12 is quite different from that given in Fig. 11 for the

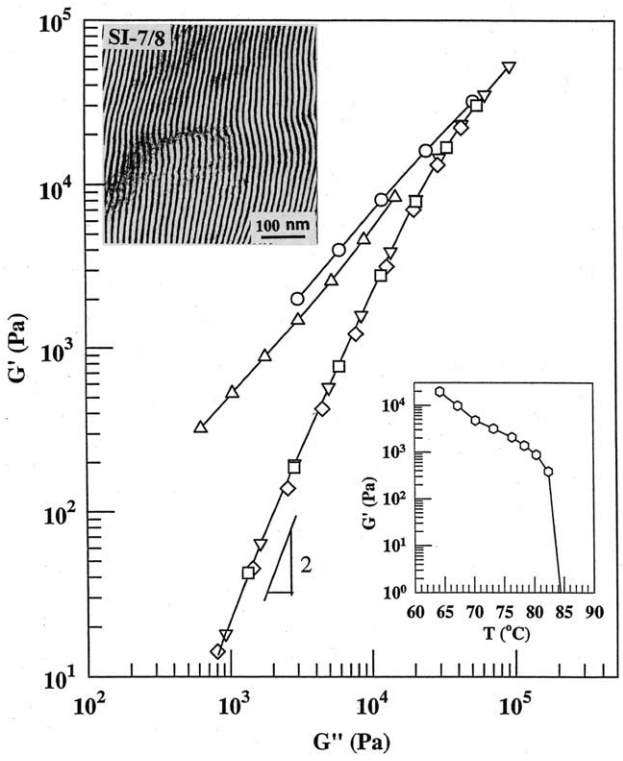

Fig. 11. Han plots for SI-7/8 at various temperatures: (○) 76 °C; (△) 83 °C; (□) 85 °C; (▽) 90 °C; (◇) 96 °C. The inset in the lower right corner gives the dependence of G' on temperature during the isochronal temperature sweep experiment at $\omega = 0.01$ rad/s in the heating cycle, and the inset in the upper left corner gives a TEM image of an SI-7/8 specimen annealed at 76 °C for 15 days. The specimen was annealed at 70 °C for 5 days. The specimens used for the rheological measurements were annealed in a vacuum at 70 °C for 5 days.

neat block copolymer SI-7/8. As was the case for the 90/10 (SB-9/8)/(PB-12) blend shown in Fig. 5, the addition of PI-14 to the nearly symmetric diblock copolymer SI-7/8 has induced LDOT and DMT. Again, the temperature at which the value of G' begins to drop rapidly at 76 °C in the plot of log G' versus temperature (see the inset of Fig. 12) almost coincides with the temperature at which the Han plot begins to have a parallel feature at 80 °C. Thus, we conclude that the isochronal dynamic temperature sweep experiment for the 90/10 (SI-7/8)/(PI-14) blend enables us to determine T_{LDOT} and not T_{DMT}. This conclusion is very similar to the conclusion drawn for the 90/10 (SB-9/8)/(PB-12) blend shown in Fig. 5. Note that the molecular weight ($M_n = 1.41 \times 10^4$ g/mol) of added homopolymer PI-14 is much higher than the molecular weight ($M_n = 7.49 \times 10^3$ g/mol) of PI block in SI-7/8 (Table 1), giving rise to $V_H/V_C = 1.05$ for (SI-7/8)/(PI-14) binary blends (Table 3).

Fig. 13 shows a temperature–composition phase diagram for (SI-7/8)/(PI-14) binary blends, where H denotes the homogeneous phase in which disordered SI-7/8 chains and PI-14 chains are mixed on a segmental level, DM denotes disordered micelles, the symbol ○ represents T_{DMT} separating the boundary between phases H and DM, and the symbol

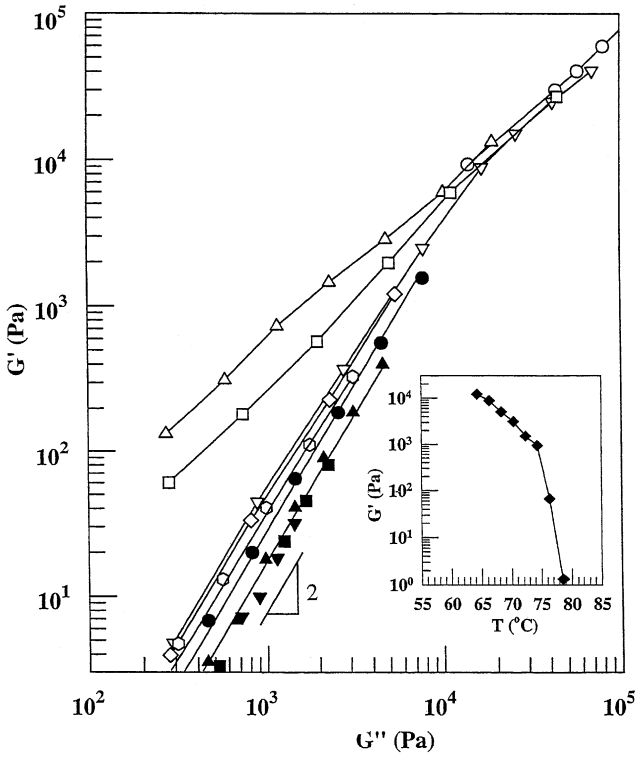

Fig. 12. Han plots for 90/10 (SI-7/8)/(PI-14) blend at various temperatures: (○) 60 °C; (△) 73 °C; (□) 77 °C; (▽) 80 °C; (◇) 90 °C; (⬡) 100 °C; (●) 108 °C; (▲) 114 °C; (■) 120 °C; (▼) 125 °C. The inset in the lower right corner gives the dependence of G' on temperature during the isochronal temperature sweep experiment at $\omega = 0.01$ rad/s in the heating cycle. The specimen was annealed at 70 °C for 5 days.

△ represents T_{LDOT} separating the boundary between phases M_1 and DM, where M_1 denotes the mesophase of SI-7/8 in which added PI-14 is solubilized. The readers are reminded that SI-7/8 has a 0.43 volume fraction of PS block (Table 1), giving rise to lamellar microdomain structure (Fig. 11). It should be mentioned that the mesophase M_1 shown in Fig. 13 may have a microdomain structure other than the lamellar microdomain structure of SI-7/8, depending upon the amount of PI-14 solubilized. That is, the addition of PI-14 to the lamella-forming diblock copolymer SI-7/8 might have induced an order–order transition from lamellae to cylindrical microdomain structure and then to spherical microdomain structure of PS phase in the PI matrix, depending upon the amount of PI-14 solubilized.

As the molecular weight of added PI is increased from 1.41×10^4 to 2.76×10^4 g/mol (Table 2), the shape of phase diagram becomes drastically different, as can be seen in Fig. 14 for (SI-7/8)/(PI-28) binary blends, where H denotes the homogeneous phase in which disordered SI-7/8 chains and PI-28 chains are mixed on a segmental level, L_1 denotes disordered SI-7/8, and L_2 denotes macrophase-separated PI-28, the symbol ○ represents T_{DMT} separating the boundary between phases H and DM, and the symbol △ represents T_{LDOT} separating the boundary between phases M_1 and DM, where M_1 denotes the mesophase of SI-7/8 in which part of

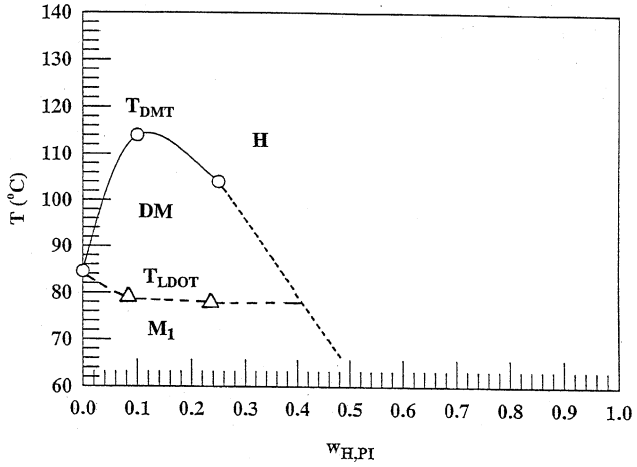

Fig. 13. Temperature–composition phase diagram for (SI-7/8)/(PI-14) blends, where H denotes the homogeneous phase in which disordered SI-7/8 chains and PI-14 chains are mixed on a molecular level, DM denotes disordered micelles, and M_1 denotes a mesophase in which part of the added PI-14 is solubilized in the microdomains of SI-7/8. The symbol ○ denotes T_{DMT} and the symbol △ denotes T_{LDOT}. No evidence of macrophase separation was observed over the entire range of blend compositions.

added PI-28 is solubilized. It should be mentioned that the mesophase M_1 shown in Fig. 14 may have a microdomain structure other than the lamellar microdomain structure of SI-7/8, depending upon the amount of PI-28 solubilized. For instance, the addition of 20 wt% PI-28 to the lamella-forming diblock copolymer SI-7/8 might have induced an order–order transition from lamellae to cylindrical microdomains of PS phase in the PI matrix. In Fig. 14, region $(M_1 + L_2)$ represents a two-phase mixture where phases M_1 and L_2 coexist, and region $(L_1 + L_2)$ represents a two-phase mixture where phases L_1 and L_2 coexist. The phase boundary between the $(M_1 + L_2)$ and $(L_1 + L_2)$ regions indicated by the dotted horizontal line in Fig. 14 is drawn with the stipulation that the mesophase M_1 in the region $(M_1 + L_2)$ would transform into the disordered phase (L_1), which coexists with macrophase-separated PI-28 phase (L_2). The phase boundary between the M_1 and $(M_1 + L_2)$ regions indicated by the solid vertical line in Fig. 14 is drawn on the basis of our light scattering experimental observation that macrophase separation occurred at 40 °C for a 0.20 weight fraction of PI-28.

The construction of the entire binodal curve over the entire composition range in Fig. 14 was not feasible, because the molecular weight of PI-28 was too high, giving rise to thermal degradation/crosslinking reactions in the homopolymer PI-28 and PI block in SI-7/8 at temperatures higher than about 240 °C. In view of the fact that the molecular weight ($M_n = 2.76 \times 10^4$ g/mol) of added homopolymer PI-28 is much higher than the molecular weight ($M_n = 7.49 \times 10^3$ g/mol) of PI block in SI-7/8 (Table 1), the addition of 10 wt% PI-28 to SI-7/8 is expected to increase the T_{DMT} of the 90/10 (SI-7/8)/(PI-28) blend over the T_{ODT} of SI-7/8. Note in Fig. 14 that the onset of

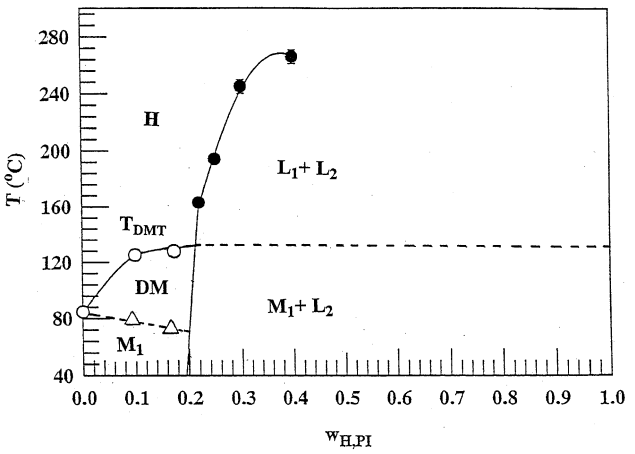

Fig. 14. Temperature–composition phase diagram for (SI-7/8)/(PI-28) blends, where H denotes the homogeneous phase in which disordered SI-7/8 chains and PI-28 chains are mixed on a molecular level, DM denotes disordered micelles, M_1 denotes a mesophase in which part of the added PI-28 is solubilized in the microdomains of SI-7/28, L_1 denotes disordered SI-7/8, and L_2 denotes macrophase-separated PI-28. The symbol ○ denotes T_{DMT}, the symbol △ denotes T_{LDOT}, and the symbol ● denotes cloud point.

macrophase separation of PI-28 occurs at $w_{H,PI} = 0.2$ ($w^T_{PS} = 0.38$), which is a manifestation of the solubility limit of PI-28 in the lamellar microdomains of PI in SI-7/8. As can be seen in Table 3, the V_H/V_C ratio is increased from 1.05 to 2.1 as $M_{H,PI}$ is increased from 1.41×10^4 to 2.76×10^4 g/mol. In view of the fact that the solubility limit of a homopolymer in a block copolymer is expected to decrease with an increase in $M_{H,A}/M_{C,A}$ ratio, it is not surprising to observe that macrophase separation in (SI-7/8)/(PI-28) binary blends occurs at $w_{H,PI} = 0.2$ (Fig. 14), whereas no macrophase separation in (SI-7/8)/(PI-14) binary blends occurs (Fig. 13).

3.6. Effect of the molecular weight of homopolymer and block copolymer composition on temperature–composition phase diagram

In order to explain the effects of $M_{H,A}/M_{C,A}$ ratio and f_{PS} on the phase behavior of block copolymer/homopolymer blends, let us examine the boundary between phases DM and H for different pairs of blends that were considered in this study. The T_{DMT} of (SI-7/29)/(PS-2) binary blends (Fig. 10) initially increases fast as the amount of PS-2 is increased to ca. 17 wt% and then tends to level off until meeting the binodal curve at B, while the T_{DMT} of (SI-7/29)/(PS-1) binary blends (Fig. 8) increases moderately as the amount of PS-1 is increased to ca. 40 wt% and then shows a moderate fall upon further addition of PS-1. This difference in phase behavior between the two blend systems for the same block copolymer can be explained by the difference in molecular weights of added homopolymers. Specifically, for SI-7/29 with $f_{PS} = 0.16$, $V_H/V_C = 0.04$ for (SI-7/29)/(PS-1) binary blends and $V_H/V_C = 0.05$ for (SI-7/29)/(PS-2) binary blends (Table 3). The above experimental observations indicate that the addition of a small amount of PS-1 or PS-2 to SI-7/29 would increase the T_{DMT} of the resulting blends and that the addition of a small amount of PS-2 having $M_n = 1.9 \times 10^3$ g/mol to SI-7/29 would increase the T_{DMT} of the resulting blend faster than the addition of a small amount of PS-1 having $M_n = 1.5 \times 10^3$ g/mol would do. Thus, we can conclude that a relatively small increase in M_n from 1.5×10^3 to 1.9×10^3 g/mol has a very large effect on the T_{DMT} of (SI-7/29)/PS binary blends having a *highly asymmetric* block copolymer SI-7/29 with spherical microdomains ($f_{PS} = 0.16$). In the case of (SI-7/8)/PI binary blends, the addition of 10 wt% PI-14 increases the T_{DMT} of the resulting 90/10 (SI-7/8)/PI-14 blend to 114 °C, and the addition of 10 wt% PI-28 increases the T_{DMT} of the resulting 90/10 (SI-7/8)/ PI-28 blend to 125 °C. Note that SI-7/8 has $T_{ODT} = 85$ °C (Table 1). Further note that $V_H/V_C = 1.05$ for (SI-7/8)/(PI-14) binary blends and $V_H/V_C = 2.10$ for (SI-7/8)/ (PI-28) binary blends (Table 3). We observe that the T_{DMT} of (SI-7/8)/PI binary blends increases only moderately (11 °C) as M_n is increased from 1.41×10^4 to 2.76×10^4 g/mol for a nearly symmetric block copolymer SI-7/8 having lamellar microdomains ($f_{PS} = 0.43$). The above observations indicate that the block copolymer composition also plays an important role in determining the phase behavior of block copolymer/homopolymer blends.

4. Concluding remarks

In this paper we have presented experimental temperature–composition phase diagrams, determined from oscillatory shear rheometry and cloud point measurements, for six pairs of SI/PS, SI/PI, SB/PS, and SB/PB binary blends, where the block copolymer has spherical or lamellar microdomain structure. We have investigated how the block copolymer composition and the molecular weight ratio of homopolymer to corresponding block ($M_{H,PS}/M_{C,PS}$, $M_{H,PI}/M_{C,PI}$, or $M_{H,PB}/M_{C,PB}$) influence the shape of temperature–composition phase diagram for the block copolymer/homopolymer blends investigated. Specifically, we have found that a small change in $M_{H,PS}/M_{C,PS}$ ratio has a large influence on the shape of temperature–composition phase diagrams of SI/PS binary blends when the SI diblock copolymer is highly asymmetric in composition, while even a large change in $M_{H,PS}/M_{C,PS}$ ratio has only a moderate influence on the shape of temperature–composition phase diagrams of SI/PS binary blends when the SI diblock copolymer is *symmetric* or *nearly symmetric* in composition.

In this study we have found that the addition of PI to a lamella-forming SI diblock copolymer or the addition of PB to a lamella-forming SB diblock copolymer induced LDOT and DMT. In this paper we have presented experimental temperature–composition phase diagrams that contain a region where DM exist. Table 4 gives a summary of the T_{LDOT} and T_{DMT} determined for three different pairs of

Table 4
Summary of T_{LDOT} and T_{DMT} for the block copolymer/homopolymer blends investigated

Sample code	T_{ODT} (°C)	T_{LDOT} (°C)	T_{DMT} (°C)
(a) SB-9/8[a]	123		
90/10 (SB-9/8)/(PB-12)		101	151
75/25 (SB-9/8)/(PB-12)		90	136
65/35 (SB-9/8)/(PB-12)		102	120
(b) SI-7/8[b]	85		
90/10 (SI-7/8)/(PI-14)		80	114
75/25 (SI-7/8)/(PI-14)		80	104
90/10 (SI-7/8)/(PI-28)		80	125
82/18 (SI-7/8)/(PI-28)		75	130
(c) SI-7/29[c]		98	135
80/20 (SI-7/29)/(PS-1)		93	146
60/40 (SI-7/29)/(PS-1)		111	142
43/57 (SI-7/29)/(PS-1)		107	140
83/17 (SI-7/29)/(PS-2)		108	161
66/34 (SI-7/29)/(PS-2)		129	164

[a] Lamella-forming SB diblock copolymer.
[b] Lamella-forming SI diblock copolymer.
[c] Sphere-forming SI diblock copolymer.

block copolymer and homopolymer investigated in this study.

We are not aware of any theoretical studies that have reported on phase diagrams for (A-*block*-B)/A or (A-*block*-B)/B binary blends, exhibiting disordered micelle region, and on phase transition from lamellar microdomains to DM when homopolymer PI is added to a lamella-forming SI diblock copolymer or when homopolymer PB is added to a lamella-forming SB diblock copolymer. In this regard, the experimental composition–temperature phase diagrams, together with the molecular parameters of the component polymers, presented in this paper will be very useful to future theoretical development predicting phase diagrams of binary blends of block copolymer and homopolymer.

Acknowledgements

We gratefully acknowledge that Dr Adel Halasa at Goodyear Tire and Rubber Company supplied us with the SB-9/8 and PB-12 employed in this study.

References

[1] Toy L, Ninomi M, Shen MJ. Macromol Sci Phys 1975;B11(3):281.
[2] Ninomi M, Akovali G, Shen MJ. Macromol Sci Phys 1977;B13(1):133.
[3] Kinning DJ, Winey KI, Thomas EL. Macromolecules 1988;21:3502.
[4] Kinning DJ, Thomas EL, Fetters LJ. J Chem Phys 1988;90:5806.
[5] Hashimoto T, Tanaka H, Hasegawa H. Macromolecules 1990;23:4378.
[6] Tanaka H, Hasegawa H, Hashimoto T. Macromolecules 1991;24:240.
[7] Tanaka H, Hashimoto T. Macromolecules 1991;24:5713.
[8] Winey KI, Thomas EL, Fetters LJ. J Chem Phys 1991;95:9367.
[9] Winey KI, Thomas EL, Fetters LJ. Macromolecules 1992;25:422.
[10] Winey KI, Thomas EL, Fetters LJ. Macromolecules 1992;25:2645.
[11] Koizumi S, Hasegawa H, Hashimoto T. Macromol Chem, Macromol Symp 1992;62:75.
[12] Hashimoto T, Koizumi S, Hasegawa H, Izumitani T, Hyde ST. Macromolecules 1992;25:1433.
[13] Disko MM, Liang KS, Behal SK, Roe RJ, Jeon KJ. Macromolecules 1993;26:2983.
[14] Spontak RJ, Smith SD, Ashraf A. Macromolecules 1993;26:956.
[15] Spontak RJ, Smith SD, Ashraf A. Macromolecules 1993;26:5118.
[16] Zin W-C, Roe R-J. Macromolecules 1984;17:183.
[17] Owens JN, Gancarz IS, Koberstein JT, Russell TP. Macromolecules 1989;22:3388.
[18] Kim J, Han CD, Chu SG. J Polym Sci, Polym Phys Ed 1988;26:677.
[19] Han CD, Kim J, Baek DM. J Adhes 1989;28:201.
[20] Han CD, Kim J, Baek DM, Chu SG. J Polym Sci, Polym Phys Ed 1990;28:315.
[21] Han CD, Baek DM, Kim J, Kimishima K, Hashimoto T. Macromolecules 1992;25:3052.
[22] Roe R-J, Zin W-C. Macromolecules 1984;17:189.
[23] Jeon KJ, Roe R-J. Macromolecules 1994;27:2439.
[24] Baek DM, Han CD, Kim JK. Polymer 1992;33:4821.
[25] Löwenhaupt B, Steurer A, Hellmann GP, Gallot Y. Macromolecules 1994;27:908.
[26] Leibler L, Benoit H. Polymer 1981;2:195.
[27] Hong KM, Noolandi J. Macromolecules 1983;16:1083.
[28] Whitmore MD, Noolandi J. Macromolecules 1985;18:2486.
[29] Nojima S, Roe R-J. Macromolecules 1987;20:1866.
[30] Banaszak M, Whitmore MD. Macromolecules 1992;25:2757.
[31] Kang C-K, Zin W-C. Macromolecules 1992;25:3039.
[32] Semenov AN. Macromolecules 1993;26:2273.
[33] Matsen MW. Macromolecules 1995;28:5765.
[34] Janert PK, Schick M. Macromolecules 1998;31:1109.
[35] Neumann C, Loveday DR, Abetz V, Stadler R. Macromolecules 1998;31:2493.
[36] Han CD, Kim J. J Polym Sci, Polym Phys Ed 1987;25:1741.
[37] Han CD, Kim J, Kim JK. Macromolecules 1989;22:383.
[38] Han CD, Baek DM, Kim JK. Macromolecules 1990;23:561.
[39] Han CD, Jhon MS. J Appl Polym Sci 1986;32:3809.
[40] Han CD, Kim JK. Macromolecules 1989;22:4292.
[41] Gouinlock EV, Porter RS. Polym Engng Sci 1977;17:534.
[42] Chung CI, Lin MI. J Polym Sci, Polym Phys Ed 1978;16:545.
[43] Widmaier JM, Meyer GC. J Polym Sci, Polym Phys Ed 1980;18:217.
[44] Han CD, Baek DM, Kim JK, Ogawa T, Sakamoto N, Hashimoto T. Macromolecules 1995;28:5043.
[45] Han CD, Vaidya NY, Kim D, Shin G, Yamaguchi D, Hashimoto T. Macromolecules 2000;33:3767.